

# CrossNet: Leveraging Global, Cross-Band, Narrow-Band, and Positional Encoding for Single- and Multi-Channel Speaker Separation

Vahid Ahmadi Kalkhorani, DeLiang Wang, *Fellow, IEEE*

**Abstract**—We introduce CrossNet, a complex spectral mapping approach to speaker separation and enhancement in reverberant and noisy conditions. The proposed architecture comprises an encoder layer, a global multi-head self-attention module, a cross-band module, a narrow-band module, and an output layer. CrossNet captures global, cross-band, and narrow-band correlations in the time-frequency domain. To address performance degradation in long utterances, we introduce a random chunk positional encoding. Experimental results on multiple datasets demonstrate the effectiveness and robustness of CrossNet, achieving state-of-the-art performance in tasks including reverberant and noisy-reverberant speaker separation. Furthermore, CrossNet exhibits faster and more stable training in comparison to recent baselines. Additionally, CrossNet’s high performance extends to multi-microphone conditions, demonstrating its versatility in various acoustic scenarios.

**Index Terms**—Complex spectral mapping, speaker separation, time-frequency domain, single-channel, multi-channel.

## I. INTRODUCTION

IN human and machine speech communication, the presence of acoustic interference, such as background noise or competing speakers, presents a considerable challenge for speech understanding. To address these challenges, speech separation systems have been developed to separate target speech signals from noisy and reverberant environments. Speech separation includes speaker separation and speech enhancement [1]. The task of speaker separation is to separate the speech signals of multiple speakers and speech enhancement aims to separate a single speech signal from nonspeech background noise. Both tasks are essential for various applications, including hearing aids, teleconferencing, and voice-controlled assistants.

Significant strides have been made in monaural talker-independent speaker separation with the introduction of deep clustering [2] and permutation invariant training (PIT) [3]. By effectively tackling the permutation ambiguity issue inherent in talker-independent training, these approaches have substantially elevated speaker separation performance. Subsequent developments have produced impressive performance gains.

For example, deep CASA [4] breaks down the speaker separation task into two phases: simultaneous grouping and sequential grouping. Conv-TasNet [5] operates on short windows

of signals and performs end-to-end masking-based separation. DPRNN [6] segments a time-domain signal into fixed-length blocks, where intra- and inter-block recurrent neural networks (RNNs) are applied iteratively to facilitate both local and global processing. SepFormer [7] replaces RNNs with a set of multi-head self-attentions (MHAs) and linear layers. Like Conv-TasNet, SepFormer is a masking approach in the time domain. The availability of spatial information from multiple microphones allows for location-based training to resolve the permutation ambiguity issue, which further improves speaker separation results [8].

While most of the effective monaural speaker separation algorithms operate in the time domain, recently, deep neural networks (DNNs) operating in the frequency domain have gained prominence by harnessing various forms of spectral information, including full-band/cross-band and sub-band/narrow-band for both single- and multi-channel speech separation. The representative model of TF-GridNet [9] employs cross-band and narrow-band long short-term memory (LSTM) networks in conjunction with a cross-frame self-attention module to perform complex spectral mapping [10]–[13]. The most effective TF-GridNet model comprises a two-stage DNN with a neural beamformer positioned in the intermediate stage. This model has strongly improved speech separation results in a variety of single-channel and multi-channel tasks. SpatialNet [14] shares a foundational framework with TF-GridNet, but employs a combination of a Conformer narrow-band block and a convolutional-linear cross-band block. Notably, SpatialNet excludes any LSTM or RNN layers. Furthermore, SpatialNet operates as a single-stage network and exhibits a more stable training trajectory, especially under conditions involving half-precision (16-bit) training. SpatialNet demonstrates very competitive results in multi-channel speaker separation. But its utility is primarily tailored for multi-channel scenarios, given its substantial reliance on spatial information afforded by microphone arrays. Another notable limitation of SpatialNet, in comparison to TF-GridNet, is its performance degradation with increasing sequence length, as recently reported in [15].

To overcome the aforementioned shortcomings and further enhance the performance of complex spectral mapping for speaker separation, we examine the underlying reasons behind the observed performance differences between TF-GridNet and SpatialNet, particularly in scenarios involving monaural separation and long utterances. We attribute the observed performance degradation of SpatialNet relative to TF-GridNet to two primary factors. First, the self-attention module within

Vahid Ahmadi Kalkhorani is with the Department of Computer Science and Engineering, The Ohio State University, Columbus, OH 43210 USA (e-mail: ahmadikalkhorani.1@osu.edu). DeLiang Wang is with the Department of Computer Science and Engineering, and the Center for Cognitive and Brain Sciences, The Ohio State University, Columbus, OH 43210 USA (e-mail: dwang@cse.ohio-state.edu).

TF-GridNet operates as a global attention mechanism, whereas SpatialNet processes each frequency independently, unable to benefit from cross-frequency and hidden features. We believe that the lack of such global attention contributes to SpatialNet's diminished performance in processing long sequences. Second, RNNs as exemplified by LSTM possess the capability to implicitly extract positional information [16]–[18]. Therefore, even though neither SpatialNet nor TF-GridNet architecture explicitly incorporates positional encoding (PE), the use of RNNs captures positional cues in TF-GridNet implicitly.

In this study, we propose a new DNN architecture, called CrossNet, for single- and multi-channel speaker separation. Building upon complex spectral mapping and the SpatialNet framework, we make the following contributions:

- We present a new DNN architecture for both single- and multi-channel speaker separation tasks. This architecture employs a global multi-head self-attention module to capture cross-frequency and cross-embedding correlations.
- We introduce a novel positional encoding method to CrossNet to address the out-of-distribution problem of common PE methods.
- CrossNet advances the state-of-the-art speaker separation performance on multiple benchmark datasets. In addition, superior results are achieved with a reduced computational overhead in terms of both inference and training time.

The rest of the paper is organized as follows. Section II describes the single- and multi-channel speaker separation problem in the time-frequency (T-F) domain. The detailed description of CrossNet is given in Section III. Section IV presents the experimental setup. Evaluation and comparison results are provided in Section V. Concluding remarks are given in Section VI.

## II. PROBLEM STATEMENT

For a mixture of  $C$  speakers in a noisy-reverberant environment captured by an array of  $M$  microphones, the recorded mixture in the time domain  $\mathbf{y}(n) \in \mathbb{R}^M$  can be modeled in terms of the direct-path signals  $\mathbf{s}_c(n) \in \mathbb{R}^M$ , their reverberations  $\mathbf{h}_c(n) \in \mathbb{R}^M$ , and reverberant background noises  $\mathbf{v}(n) \in \mathbb{R}^M$

$$\mathbf{y}(n) = \sum_{c=1}^C (\mathbf{s}_c(n) + \mathbf{h}_c(n)) + \mathbf{v}(n) \quad (1)$$

where  $n$  denotes discrete time and  $c$  indexes speakers. In the short-time Fourier transform (STFT) domain, the model is expressed as:

$$\mathbf{Y}(t, f) = \sum_{c=1}^C (\mathbf{S}_c(t, f) + \mathbf{H}_c(t, f)) + \mathbf{V}(t, f) \quad (2)$$

where  $t$  indexes time frames and  $f$  frequency bins.  $\mathbf{Y}(t, f)$ ,  $\mathbf{S}_c(t, f)$ ,  $\mathbf{H}_c(t, f)$ , and  $\mathbf{V}(t, f) \in \mathbb{C}^M$  denote the complex spectrograms of the mixture, the direct-path signal and its reverberation of speaker  $c$ , and background noise, respectively.

The goal of complex spectral mapping based speaker separation is to train a DNN to estimate the real and imaginary parts of the direct-path signal of each speaker  $\mathbf{S}_c(t, f)$  from the mixture  $\mathbf{Y}(t, f)$ . We can turn the general formulation in (2) to more specific forms by restricting certain parameters and terms. In the case of monaural, anechoic speaker separation,  $C > 1$ ,  $M = 1$ , both  $\mathbf{H}_c(t, f)$  and  $\mathbf{V}(t, f)$  are absent. In reverberant speaker separation,  $C > 1$  and  $\mathbf{V}(t, f)$ , if present, represents a weak noise. In the case of noisy-reverberant speaker separation,  $C > 1$  and  $\mathbf{V}(t, f)$  includes significant background noise.

## III. CROSSNET

The diagram of the proposed system is provided in Fig. 1. CrossNet comprises an encoder layer, a global multi-head self-attention (GMHSA) module, a cross-band module, a narrow-band module, and a decoder layer. To ensure comparable energy levels for all signals processed by CrossNet, we normalize the input signal by its variance before processing its samples. In the multi-channel setup, we normalize the signals from all microphones by the variance of the reference microphone; the same variance is applied to restore the scale of a predicted signal. Then, we apply STFT to the normalized signal and stack the real and imaginary (RI) parts. For the multi-channel setup, we stack the RI parts from all microphones as done in neural spectrospatial filtering [19]. The stacked RI parts are sent to the encoder layer, which learns to extract acoustic features from the input in the STFT domain. The global multi-head self-attention module captures global correlations, while the cross-band module captures cross-band correlations. The narrow-band module focuses on capturing information at neighboring frequency bins. Finally, the output layer maps the separated features to a T-F representation, which is then converted back to the time domain using inverse short-time Fourier transform (iSTFT).

### A. Encoder layer

The encoder is a 1D convolutional layer (Conv1D) layer with a kernel size of  $k$  and a stride of 1. The encoder layer converts the input T-F domain signal from  $M \times F \times T$  to  $H \times F \times T$  where  $H$  is the number of hidden channels.  $F$  is the number of frequency bins and  $T$  is number of frames.

### B. Random chunk positional encoding

To address the limitation of separation methods in dealing with long utterances, we introduce a PE method, called random-chunk positional encoding (RCPE), to tackle the out-of-distribution problem in positional encoding approaches. RCPE is inspired by random positional encoding recently proposed for natural language processing [20]. Transformers demonstrate impressive generalization capabilities on learning tasks with a fixed context length. However, their performance degrades when tested on longer sequences than the maximum length encountered in training. This degradation is attributed to the fact that positional encoding becomes out-of-distribution for longer sequences, even for relative positional encoding

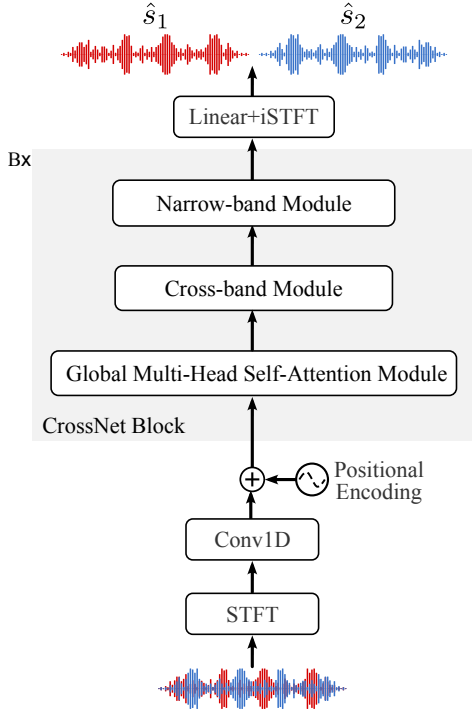


Fig. 1: Diagram of the proposed CrossNet architecture, with  $\hat{s}_1$  and  $\hat{s}_2$  denoting separated speaker signals.

[20]. RCPE selects a contiguous chunk of positional embedding vectors from a pre-computed PE matrix during training. For RCPE, we start by defining PE as a combination of sine and cosine functions [21] as

$$\text{PE}(t, 2i) = \sin\left(\frac{t}{10000^{2i/(F \times H)}}\right) \quad (3a)$$

$$\text{PE}(t, 2i + 1) = \cos\left(\frac{t}{10000^{2i/(F \times H)}}\right) \quad (3b)$$

When the model is in the training mode, we select a random chunk from index  $\tau$  to index  $\tau + T - 1$ , where  $\tau$  is drawn randomly from  $[1, T^{\max} - T + 1]$ , with  $T^{\max}$  denoting the maximum desired sequence length during inference. When the model is in test or validation mode, we select the first  $T$  embedding vectors. Finally, we add the selected PEs to the input features. We obtain positional encoding vectors as

$$\text{RCPE}(T) = \begin{cases} \text{PE}[\tau : \tau + T - 1, \dots] & \text{if training} \\ \text{PE}[1 : T - 1, \dots] & \text{else} \end{cases} \quad (4)$$

This technique allows the CrossNet model to see all possible positional embedding vectors during the training stage while maintaining the relative distance between embeddings, thus improving generalization to longer sequences. Additionally, RCPE has no learnable parameter and has a negligible computational cost.

### C. Global multi-head self-attention module

Fig. 2(a) shows the diagram of the global multi-head self-attention module. In TF-GridNet [9], the cross-frame self-attention module employs three point-wise convolution layers

for frame-level feature extraction of queries, keys, and values. In contrast, we utilize a single convolution layer with  $L(2E + H/L)$  output channels to extract frame-level features from T-F embeddings. Subsequently, we split the result into  $L$  queries  $Q^l \in \mathbb{R}^{E \times F \times T}$ , keys  $K^l \in \mathbb{R}^{E \times F \times T}$ , and values  $V^l \in \mathbb{R}^{H/L \times F \times T}$ . Here,  $E$  represents the output channel dimension of the point-wise convolution and  $l$  indexes the head number. This method avoids the sequential operations of the three Conv1D layers, which can be computationally expensive. Subsequently, a self-attention layer is applied to these embeddings to capture global correlations. The results of all heads are concatenated and passed to another point-wise convolution with an output dimension of  $D$  followed by a parametric rectified linear unit (PReLU) activation function and layer normalization (LN). We add this value to the input of the GMHSA module to obtain the output of the module. Note that, compared to [14] where the MHA module acts on each frequency bin separately, we first merge all frequency features into the channel dimension and then apply MHA. This method allows each frame to attend to any frame of interest in all feature channels, facilitating the exploitation of long-range correlations in both frequency and hidden feature channels.

### D. Cross-band module

To capture cross-band correlations within the input signal, we adopt the cross-band module proposed in [14]. This module, illustrated in Fig. 2(b), integrates two frequency-convolutional modules and a full-band linear module. The frequency-convolutional module aims to capture correlations between neighboring frequencies. This module includes an LN layer, a grouped convolution layer along the frequency axis (F-GConv1d), and a PReLU activation function. In the full-band linear module, we first employ a linear layer followed by sigmoid-weighted linear unit (SiLU) activation function to reduce the number of hidden channels from  $H$  to  $H'$ . Then, we apply a set of linear layers along the frequency axis to capture full-band features. Each feature channel has a dedicated linear layer denoted as  $\text{Linear}_i$  for  $i = 1, \dots, H'$ , as shown in Fig. 2(b). Note that the parameters of these layers are shared among all CrossNet blocks. Finally, the output of the module is obtained by increasing the number of channels back to  $H$  using a linear layer with SiLU activation and adding to the original input of this module.

### E. Narrow-band module

As illustrated in Fig. 2(c), the narrow-band module is composed of a layer normalization (LN), a linear layer followed by a SiLU activation, a time-convolutional (T-Conv) layer, and a final linear layer. The first linear layer in this module increases the number of features in the input from  $H$  to  $H''$  and the last linear layer converts the feature dimension back to  $H$ .

T-Conv is composed of three grouped 1d convolution (T-GConv1D) layers followed by a SiLU activation function. The second T-GConv1D is followed by a grouped normalization layer. The narrow-band module is a modified version of the Conformer convolutional block [22]. Compared to SpatialNet's

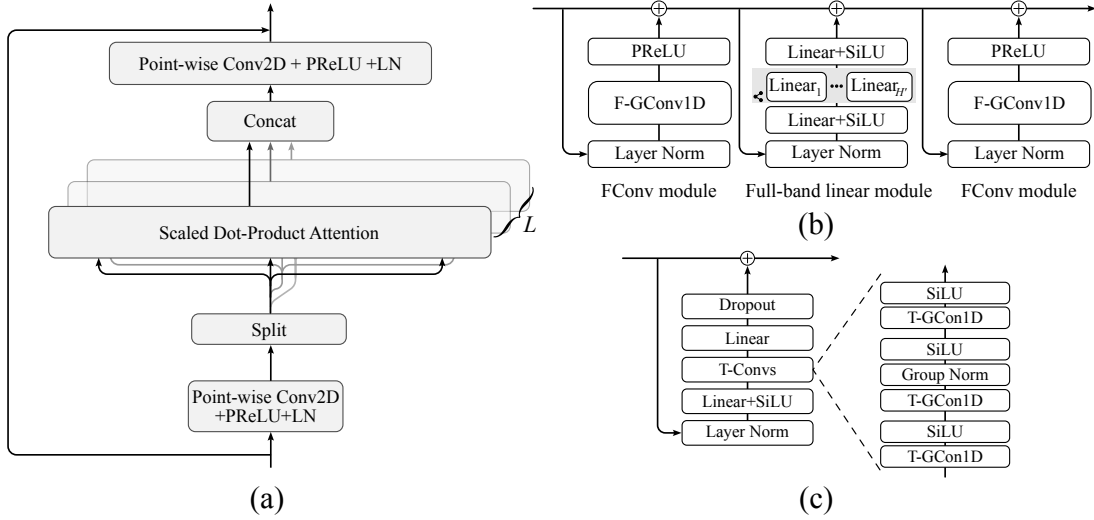


Fig. 2: CrossNet building blocks. (a) Global multi-head self-attention module. (b) Cross-band module. (c) Narrow-band module.

narrow-band block, we remove the MHA module as narrow-band correlations are captured in the GMHSA module of CrossNet.

#### F. Output layer

We use a linear output layer to map the processed features from the final CrossNet block to the predicted RI parts of each talker. Subsequently, we obtain the time-domain separated speech signals by performing the iSTFT. As mentioned at the beginning of Section III, we multiply the estimated target signals by the variance of the input mixture to ensure that their energy levels are consistent with the mixture level.

#### G. Loss functions

We use the scale-invariant signal-to-distortion ratio (SI-SDR) [23] loss function  $\mathcal{L}_{\text{SI-SDR}}$  to train CrossNet on the WSJ0-2mix dataset [2]. For training on other datasets, we employ a combination of magnitude loss  $\mathcal{L}_{\text{Mag}}$  and SI-SDR loss  $\mathcal{L}_{\text{SI-SDR}}$ , similar to [9]. We use the standard form of SI-SDR where the target signal is scaled to match the scale of the estimated signal. Also, we scale the magnitude loss by the  $L_1$  norm of the magnitude of the target signal in the STFT domain similar to [24]. These loss functions are defined below

$$\mathcal{L} = \mathcal{L}_{\text{Mag}} + \mathcal{L}_{\text{SI-SDR}} \quad (5a)$$

$$\mathcal{L}_{\text{Mag}} = \frac{\| |\text{STFT}(\hat{s}_c)| - |\text{STFT}(s_c)| \|_1}{\| |\text{STFT}(s_c)| \|_1} \quad (5b)$$

$$\mathcal{L}_{\text{SI-SDR}} = - \sum_{c=1}^C 10 \log_{10} \frac{\|s_c\|_2^2}{\|\hat{s}_c - \alpha_c s_c\|_2^2} \quad (5c)$$

$$\alpha_c = \frac{s_c^T \hat{s}_c}{\hat{s}_c^T s_c} \quad (5d)$$

In the above equations,  $\|\cdot\|_1$  is the  $L_1$  norm,  $|\cdot|$  is the magnitude operator,  $\alpha_c$  is the scaling factor, and  $(\cdot)^T$  denotes the transpose operation. We employ utterance-level PIT [25] to resolve the permutation ambiguity problem during training.

## IV. EXPERIMENTAL SETUP

### A. Datasets

We assess the efficacy of the proposed CrossNet model for speaker separation under anechoic, reverberant, and noisy-reverberant environments. we use publicly available datasets, and compare with previously published results to document the relative performance.

For single-channel speaker separation in anechoic conditions, we employ the WSJ0-2mix dataset [2], which is widely used for benchmarking monaural talker-independent speaker separation algorithms. The WSJ0-2mix dataset consists of 20,000 ( $\sim 30.4$  hours), 5,000 ( $\sim 7.7$  hours), and 3,000 ( $\sim 4.8$  hours) two-speaker mixtures for training, validation, and test sets, respectively. In WSJ0-2mix, the two utterances in each mixture are fully overlapped, and their relative energy level is sampled from the range of  $[-5, 5]$  dB. Speech is sampled at a rate of 8 kHz. To make a fair comparison, similar to TF-GridNet, we do not utilize any data augmentation techniques such as dynamic-mixing [26] or speed-perturbation [7].

For joint speaker separation, denoising, and dereverberation, we employ the WHAMR! dataset [27] and the single-channel SMS-WSJ dataset [28]. WHAMR! utilizes the two-speaker mixtures from WSJ0-2mix, but introduces reverberation to each clean anechoic signal and non-stationary background noises. The dataset includes 20,000 ( $\sim 30.4$  hours), 5,000 ( $\sim 7.7$  hours), and 3,000 ( $\sim 4.8$  hours) mixtures for training, validation, and testing, respectively.

Furthermore, for both monaural and multi-channel separation in noisy and reverberant environments, we employ the SMS-WSJ dataset [28]. This simulated two-speaker mixture dataset incorporates clean speech signals from the WSJ0 corpus and simulates a six-microphone circular array with a radius of 10 cm. Room impulse responses (RIRs) are generated using the image method [29], with T60 uniformly sampled between 0.2 s and 0.5 s. Additionally, white sensor noise is added to speech mixtures with signal-to-noise ratios (SNRs) uniformly sampled in the range of 20 dB to 30 dB. The source positions are randomly sampled within 1 m to 2

m away from the array center. The signals are sampled at a rate of 8 kHz, and the dataset includes a baseline automatic speech recognition (ASR) model built from Kaldi [30].

### B. Network configuration

For our proposed CrossNet architecture, we make use of the hyperparameters in [9] and [14]. We set the kernel size of encoder layer  $k$ , time-dimension group convolution (T-GConv1d), and frequency-dimension group convolution (F-GConv1d) to 5, 5, and 3, respectively. The number of groups for T-GConv1d, F-GConv1d, and group normalization is all set to 8. The proposed model architecture comprises  $B = 12$  blocks, with hidden channel sizes set to  $H = 192$ ,  $H' = 16$ , and  $H'' = 384$ . We employ  $N = 4$  self-attention heads in the GMHSA module with an embedding dimension of  $D = 64$  and  $E = \lceil 512/F \rceil$ , where  $\lceil \cdot \rceil$  denotes ceiling operation.

To process the input data, we apply STFT using a Hanning window with frame length of 256 samples (32 ms) and frame shift of 128 samples (16 ms). The length of training utterances is fixed at 3 seconds for the WSJ0-2mix dataset and 4 seconds for the WHAMR! and SMS-WSJ datasets.

We utilize the Adam optimizer with a maximum learning rate of 0.001. We start with a cosine warm-up scheduler that increases the learning rate from  $10^{-6}$  to  $10^{-3}$  over the first 10 epochs. Following this, we switch to the PyTorch ReduceLROnPlateau scheduler, setting the patience to 3 epochs and the reduction factor to 0.9. We found that this learning rate scheduler is more stable and results in faster convergence than the exponential decay or ReduceLROnPlateau schedulers used in [14] and [9], respectively. In our experiments, we employ the half-precision (mixed-16) training strategy to reduce the memory footprint and accelerate training. We train the model until the validation loss does not improve for 10 epochs consecutively. In each case, we use the maximum number of batches that fit into the GPU memory (NVIDIA A100 GPU with 40 GB).

### C. Evaluation metrics

We employ a set of widely used objective metrics to assess the performance of CrossNet. These metrics include: SI-SDR and its improvement (SI-SDRi) [31], SDR and its improvement (SDRi) [32], narrow-band perceptual evaluation of speech quality (PESQ) [33], and extended short-time objective intelligibility (eSTOI) [34]. To compute these metrics, we utilize the TorchMetrics[audio] package [35], which offers a comprehensive set of evaluation tools specifically designed for audio tasks.

## V. EVALUATION RESULTS

### A. Ablation study on WHAMR!

Table I presents an ablation study conducted on the single-channel WHAMR! dataset. Each row represents a different configuration of the model. The columns in this table provide information about the presence of RCPE, GMHSA, and narrow-band multi-head self-attention (NB-MHSA), along with the number of trainable parameters in millions or

Params (M), and the number of Giga floating point operations (GFLOPs) per second of input audio, as well as the separation performance metrics of SI-SDR, SDR, and PESQ. For the computation of GFLOPs, we use the official tool provided by PyTorch<sup>1</sup>. The absence of RCPE and GMHSA (Row 1) results in lower SI-SDR and PESQ scores compared to the configurations where these components are present. Note that Row 1 corresponds to the architecture of SpatialNet [14]. Adding the GMHSA module in Row 2 improves SI-SDR by 1.3 dB and PESQ by 0.31, highlighting the important role of GMHSA. In the third row, we include an LSTM encoder before CrossNet blocks, which performs positional encoding implicitly. The LSTM encoder comprises two bi-directional long short-term memory (BLSTM) layers similar to TF-GridNet’s intra-frame full-band and sub-band temporal modules. Although this configuration exhibits the highest SI-SDR and PESQ values among the tested configurations, it has the largest number of parameters and the lowest computational efficiency. Including RCPE in the fourth row improves SI-SDR by 0.3 dB and PESQ by 0.07 compared to the second row, demonstrating the utility of the proposed positional encoding.

Finally, in Row 5, we remove NB-MHSA and obtain speaker separation results with only a 0.01 PESQ reduction compared to Row 4. But the configuration with no NB-MHSA has about 20% fewer trainable parameters and 33% fewer GFLOPs. This shows that the narrow-band correlations are already captured in the GMHSA module and there is little need to include both modules in the network.

TABLE I: Ablation study on the WHAMR! dataset

Row	PE	GMHSA	NB-MHSA	Params (M)	GFLOPs	SI-SDR	PESQ
1	✗	✗	✓	6.50	118.84	10.2	2.54
2	✗	✓	✓	8.35	143.51	11.5	2.85
3	LSTM	✓	✗	9.40	160.19	11.9	2.94
4	RCPE	✓	✓	8.35	143.5	11.8	2.92
5	RCPE	✓	✗	6.57	96.14	11.8	2.91

### B. WSJ0-2mix results

We first evaluate the performance of CrossNet for monaural anechoic speaker separation. The mixture SI-SDR is 0 dB, and the mixture SDR is 0.2 dB. The results are provided in Table II along with 16 other baselines. The table includes two versions of TF-GridNet, one with 8.2M parameters and another with 14.5M parameters. The original study [9] reports the 14.5M parameter version on the WSJ0-2mix dataset. To compare models of comparable sizes, we include the 8.2M variant as well. The performance of this smaller TF-GridNet model is based on a model checkpoint trained by its original first author [36]. CrossNet surpasses the performance of state-of-the-art methods, including TF-GridNet (8.2M) [9] by 0.5 dB SI-SDR and 0.6 dB SDR. Moreover, our proposed model has around 20% fewer trainable parameters compared to TF-GridNet and faster training and inference as presented in Section V-F later. Furthermore, our proposed model underwent half-precision floating-point training rather than full-precision training done

<sup>1</sup>torch.utils.flop\_counter.FlopCounterMode

in TF-GridNet, effectively reducing memory requirements and expediting the training process.

TABLE II: Speaker separation results of CrossNet and comparison methods on the WSJ0-2mix dataset

Method	Params (M)	SI-SDRi	SDRi
Conv-TasNet [5]	5.1	15.3	15.6
Deep CASA [4]	12.8	17.7	18.0
FurcaNeXt [37]	51.4	-	18.4
SUDO RM-RF [38]	2.6	18.9	-
DPRNN [6]	7.5	20.1	20.4
DPTNet [17]	2.7	20.2	20.6
DPTCN-ATPP [39]	4.7	19.6	19.9
SepFormer [7]	26.0	20.4	20.5
Sandglasset [40]	2.3	20.8	21.0
Wavesplit [26]	29.0	21.0	21.2
TFPSNet [41]	2.7	21.1	21.3
DPTNet [17]	4.0	21.5	21.7
SFSRNet [42]	59.0	22.0	22.1
QDPN [43]	200.0	22.1	-
TF-GridNet* [9]	8.2	22.8	22.9
TF-GridNet [9]	14.5	23.5	23.6
CrossNet	6.6	23.2	23.4

\*checkpoint from [36]

### C. Results on WHAMR! and single-channel SMS-WSJ datasets

The single-channel WHAMR! results are summarized in Table III. CrossNet achieves an SI-SDR of 11.8 dB, an SDR of 12.9 dB, and a PESQ of 2.91, outperforming the previous best of TF-GridNet (1-stage) [9] and TF-GridNet (2-stage) [9] by 0.16 and 0.12 PESQ, respectively. The 2-stage TF-GridNet consists of the first DNN followed by a single-channel multi-frame Wiener filter (SCMFWF) and then the second DNN. This comparison is significant as CrossNet is a single-stage model, and a 2-stage model not only has more parameters but also takes more effort to train and deploy. Our advantage can be attributed to the use of more convolutional layers, which enables CrossNet to learn filtering operations. Note that SpatialNet is not designed for single-channel separation tasks even though it can be applied to monaural separation. We include its results in Table III for reference purposes only. Compared to the results in Table II, these results underscore the advantage of CrossNet over TF-GridNet for single-channel speaker separation in noisy-reverberant conditions.

To examine the impact of SCMFWF on model performance, we train CrossNet with a similar setup to the two-stage TF-GridNet, and 2-stage CrossNet results are included in Table III. We observe a very small improvement. Thus, we conclude that two stages are not necessary and will not be further assessed for CrossNet. This observation shows that, compared to TF-GridNet where SCMFWF improves the performance, the Wiener filtering effects are already incorporated in CrossNet.

TABLE III: Speaker separation results of CrossNet and comparison methods on the WHAMR! dataset

Method	SI-SDR	SDR	PESQ	eSTOI
Unprocessed	-6.1	-3.5	1.41	0.317
Sepformer [7]	7.9	-	-	-
MossFormer [44]	10.2	-	-	-
SpatialNet (large) [14]	10.2	11.2	2.54	0.772
TF-GridNet (1-stage) [9]	10.6	11.7	2.75	0.793
TF-GridNet (2-stage) [9]	11.2	12.3	2.79	0.808
CrossNet (2-stage)	12.0	13.1	2.91	0.824
CrossNet	11.8	12.9	2.91	0.823

Table IV presents evaluation and comparison results on the single-channel SMS-WSJ dataset, including ASR results in terms of word error rate (WER) in percentage (%) evaluated on the provided ASR model. CrossNet outperforms TF-GridNet (1-stage) [9] by the substantial margin of 3.0 dB in SI-SDR and 0.29 in PESQ. Notably, CrossNet outperforms the two-stage TF-GridNet aside from the WER score.

TABLE IV: Speaker separation and ASR results on single-channel SMS-WSJ dataset

Method	SI-SDR	SDR	PESQ	eSTOI	WER
Unprocessed	-5.5	-0.4	1.50	0.441	78.40
Oracle direct-path	$\infty$	$\infty$	4.50	1.000	6.16
DPRNN-TasNet [45]	6.5	-	2.28	0.734	38.10
SISO <sub>1</sub> [46]	5.7	-	2.4	0.748	28.70
DNN <sub>1</sub> +(FCP+DNN <sub>2</sub> ) $\times$ 2 [46]	12.7	14.1	3.25	0.899	12.80
DNN <sub>1</sub> +(msFCP+DNN <sub>2</sub> ) $\times$ 2 [47]	13.4	-	3.41	-	10.90
TF-GridNet [9] (1-stage)	16.2	17.2	3.45	0.924	9.49
TF-GridNet [9] (2-stage)	18.4	19.6	3.70	0.952	7.91
CrossNet	19.2	20.2	3.74	0.953	8.35

### D. Results on multi-channel SMS-WSJ

Table V reports the performance of the six-channel speaker separation and ASR on the SMS-WSJ corpus, along with the oracle WER results. The table reveals large improvements in speech quality and ASR performance thanks to speaker separation. The time-domain end-to-end models FaSNet+TAC [48] and MC-ConvTasNet [49] show inferior performance compared to other methods, especially on the ASR task. Time-frequency methods such as MISO<sub>1</sub>-BF-MISO<sub>3</sub> [46] and TFGridNet [9] incorporate neural beamforming and post-processing, and demonstrate significantly better separation and ASR performances. Among the comparison methods, SpatialNet is the top performer, and it leverages an advanced full-band and sub-band combination network and extensively employs convolutional and linear layers that can act as a large filter. CrossNet surpasses SpatialNet and TFGridNet in speaker separation performance, e.g. by larger than 0.1 PESQ improvement. Since the original SpatialNet is trained using a different setup, to make a fair comparison, we also train the SpatialNet with the same setup as CrossNet, including the loss function and learning rate scheduler, and report the results in Table V. Even though the use of the same training

setup improves SpatialNet performance in terms of PESQ, WER, and eSTOI, it still underperforms CrossNet, e.g. by 1 dB in SI-SDR and 5.7% relative WER. CrossNet’s WER of 6.30% is remarkably close to the oracle score of 6.16%. As CrossNet has a similar architecture to SpatialNet, the superior performance of CrossNet can be attributed to the proposed positional encoding and the GMHSA module.

TABLE V: Speaker separation and ASR results on the 6-channel SMS-WSJ dataset

Method	SI-SDR	SDR	PESQ	eSTOI	WER
Unprocessed	-5.5	-0.4	1.50	0.441	78.40
Oracle direct-path	$\infty$	$\infty$	4.50	1.000	6.16
FasNet+TAC [48]	8.6	-	2.37	0.771	29.80
MC-ConvTasNet [49]	10.8	-	2.78	0.844	23.10
MISO <sub>1</sub> [46]	10.2	-	3.05	0.859	14.0
LBT [8]	13.2	14.8	3.33	0.910	9.60
MISO <sub>1</sub> -BF-MISO <sub>3</sub> [46]	15.6	-	3.76	0.942	8.30
TF-GridNet (1-stage) [9]	19.9	21.2	3.89	0.966	6.92
TF-GridNet (2-stage) [9]	22.8	24.9	4.08	0.980	6.76
SpatialNet [14]	25.1	27.1	4.08	0.980	6.70
SpatialNet <sup>◊</sup>	24.8	26.9	4.15	0.985	6.66
CrossNet	25.8	27.6	4.20	0.987	6.30

<sup>◊</sup> Trained with the same setup as CrossNet

### E. Performance over different utterance lengths

To assess the impact of utterance length on CrossNet’s performance, we plot the SI-SDR and PESQ scores across various sequence lengths on the 6-channel SMS-WSJ dataset. The results are depicted in Fig. 3. CrossNet yields better performance than SpatialNet [14] across all sequence lengths. The CrossNet model exhibits stable performance across different sequence lengths, whereas SpatialNet exhibits some degradation for long sequences, in line with the findings reported in [15], CrossNet maintains robust performance across the spectrum of sequence lengths and even produces some SI-SDR improvement for long mixtures. This performance profile highlights the contribution of the proposed positional encoding, and is important for real-world applications where the length of mixture utterances may vary significantly.

### F. Computational complexity

Finally, we document computational load in terms of GFLOPs and the number of trainable parameters in millions (Params) of CrossNet and several other methods. The complexities are tabulated in Table VI for two sampling rates of 8 and 16 kHz. The computation of GFLOPs is as outlined in [14], where GFLOPs are quantified based on a four-second audio signal captured by a 6-channel microphone array speaker. The complexities of the comparison methods are obtained from [14]. As clear from the table, CrossNet exhibits much lower complexity than TF-GridNet. Compared to SpatialNet, CrossNet has smaller GFLOPs and comparable numbers of trainable parameters.

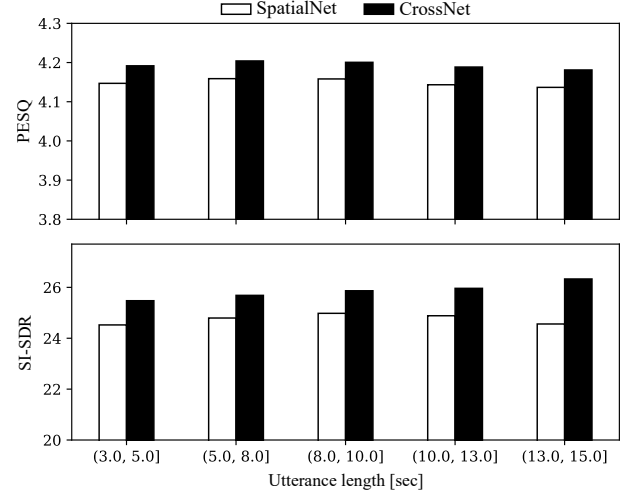


Fig. 3: Effects of sequence length on the performance of CrossNet and SpatialNet. Speaker separation performance is plotted for different intervals of mixture lengths (in seconds).

TABLE VI: Computational complexity and model size of the proposed model and comparison methods.

Model	8 kHz		16 kHz	
	GFLOPs	Params (M)	GFLOPs	Params (M)
NBDF [50]	19.5	1.2	38.9	1.2
FT-JNF [51]	19.5	1.2	38.9	1.2
McNet [52]	29.7	1.9	59.2	1.9
DasFormer [53]	33.3	2.2	76.4	2.2
TFGridNet [9]	348.4	11.0	695.6	11.2
SpatialNet [14]	119.0	6.5	237.9	7.3
CrossNet	96.3	6.6	191.7	8.2

## VI. CONCLUDING REMARKS

We have introduced CrossNet, a novel DNN architecture for single- and multi-channel speaker separation in noisy-reverberant environments. CrossNet includes an encoder layer, a global multi-head self-attention module, cross-band and narrow-band modules, and an output layer, to leverage both global and local information in an audio signal to enhance speaker separation and speech enhancement performance. The global multi-head self-attention module allows the model to attend to any frame of interest in all feature and frequency channels, facilitating the exploitation of long-range dependencies. We introduce a novel random chunk positional encoding technique to improve generalization to longer sequences. The cross-band module captures cross-band correlations within the input signal, while the narrow-band module focuses on capturing correlations at neighboring frequency bins. The evaluation experiments conducted on multiple open datasets demonstrate that CrossNet achieves state-of-the-art performance for single- and multi-channel speaker separation tasks. Moreover, CrossNet exhibits stable performance in separating multi-talker mixtures of variable lengths, and is computationally efficient compared to recently-established strong baselines.

## VII. ACKNOWLEDGEMENTS

We thank the members of the Perception and Neurodynamics Lab (PNL), especially Hassan Taherian and Heming Wang, for insightful discussions and their suggestions during the development of CrossNet. This work was supported in part by an National Science Foundation grant (ECCS-2125074), the Ohio Supercomputer Center, the NCSA Delta Supercomputer Center (OCI 2005572), and the Pittsburgh Supercomputer Center (NSF ACI-1928147).

## REFERENCES

- [1] D. Wang and J. Chen, "Supervised speech separation based on deep learning: An overview," *IEEE/ACM Trans. Audio, Speech, Lang. Process.*, vol. 26, pp. 1702–1726, 2018.
- [2] J. R. Hershey, Z. Chen, J. Le Roux, and S. Watanabe, "Deep clustering: Discriminative embeddings for segmentation and separation," in *Proc. ICASSP*, 2016, pp. 31–35.
- [3] M. Kolbæk, D. Yu, Z.-H. Tan, and J. Jensen, "Multitalker speech separation with utterance-level permutation invariant training of deep recurrent neural networks," *IEEE/ACM Trans. Audio, Speech, Lang. Process.*, vol. 25, pp. 1901–1913, 2017.
- [4] Y. Liu and D. Wang, "Divide and conquer: A deep casa approach to talker-independent monaural speaker separation," *IEEE/ACM Trans. Audio, Speech, Lang. Process.*, vol. 27, pp. 2092–2102, 2019.
- [5] Y. Luo and N. Mesgarani, "Conv-TasNet: Surpassing ideal time-frequency magnitude masking for speech separation," *IEEE/ACM Trans. Audio, Speech, Lang. Process.*, vol. 27, pp. 1256–1266, 2019.
- [6] Y. Luo, Z. Chen, and T. Yoshioka, "Dual-path RNN: efficient long sequence modeling for time-domain single-channel speech separation," in *Proc. ICASSP*, 2020, pp. 46–50.
- [7] C. Subakan, M. Ravanelli, S. Cornell, F. Grondin, and M. Bronzi, "Exploring self-attention mechanisms for speech separation," *IEEE/ACM Trans. Audio, Speech, Lang. Process.*, vol. 31, pp. 2169–2180, 2023.
- [8] H. Taherian, K. Tan, and D. Wang, "Multi-channel talker-independent speaker separation through location-based training," *IEEE/ACM Trans. Audio, Speech, Lang. Process.*, vol. 30, pp. 2791–2800, 2022.
- [9] Z.-Q. Wang, S. Cornell, S. Choi, Y. Lee, B.-Y. Kim, and S. Watanabe, "TF-GridNet: Integrating full-and sub-band modeling for speech separation," *IEEE/ACM Trans. Audio, Speech, Lang. Process.*, pp. 3221–3236, 2023.
- [10] D. S. Williamson, Y. Wang, and D. Wang, "Complex ratio masking for monaural speech separation," *IEEE/ACM Trans. Audio, Speech, Lang. Process.*, vol. 24, pp. 483–492, 2016.
- [11] S.-W. Fu, T.-y. Hu, Y. Tsao, and X. Lu, "Complex spectrogram enhancement by convolutional neural network with multi-metrics learning," in *Proc. MLSP*, 2017, pp. 1–6.
- [12] K. Tan and D. Wang, "Learning complex spectral mapping with gated convolutional recurrent networks for monaural speech enhancement," *IEEE/ACM Trans. Audio, Speech, Lang. Process.*, vol. 28, pp. 380–390, 2019.
- [13] Z.-Q. Wang and D. Wang, "Deep learning based target cancellation for speech dereverberation," *IEEE/ACM Trans. Audio, Speech, Lang. Process.*, vol. 28, pp. 941–950, 2020.
- [14] C. Quan and X. Li, "Spatialnet: Extensively learning spatial information for multichannel joint speech separation, denoising and dereverberation," *IEEE/ACM Trans. Audio, Speech, Lang. Process.*, vol. 32, pp. 1310–1323, 2024.
- [15] H. Taherian and D. Wang, "Multi-channel conversational speaker separation via neural diarization," *arXiv:2311.08630*, 2023.
- [16] J. Rosendahl, V. A. K. Tran, W. Wang, and H. Ney, "Analysis of positional encodings for neural machine translation," in *Proc. Spoken Language Translation*, 2019.
- [17] J. Chen, Q. Mao, and D. Liu, "Dual-path transformer network: Direct context-aware modeling for end-to-end monaural speech separation," *arXiv:2007.13975*, 2020.
- [18] F. Andayani, L. B. Theng, M. T. Tsun, and C. Chua, "Hybrid LSTM-transformer model for emotion recognition from speech audio files," *IEEE Access*, vol. 10, pp. 36 018–36 027, 2022.
- [19] K. Tan, Z.-Q. Wang, and D. Wang, "Neural spectrospatial filtering," *IEEE/ACM Trans. Audio, Speech, Lang. Process.*, vol. 30, pp. 605–621, 2022.
- [20] A. Ruoss, G. Delétang, T. Genewein, J. Grau-Moya, R. Csordás, M. Bannani, S. Legg, and J. Veness, "Randomized positional encodings boost length generalization of transformers," *arXiv:2305.16843*, 2023.
- [21] A. Vaswani, N. Shazeer, N. Parmar, J. Uszkoreit, L. Jones, A. N. Gomez, E. Kaiser, and I. Polosukhin, "Attention is all you need," *Adv. Neural Info. Proc. Sys.*, vol. 30, 2017.
- [22] A. Gulati, J. Qin, C.-C. Chiu, N. Parmar, Y. Zhang, J. Yu, W. Han, S. Wang, Z. Zhang, Y. Wu *et al.*, "Conformer: Convolution-augmented transformer for speech recognition," *arXiv:2005.08100*, 2020.
- [23] J. Le Roux, S. Wisdom, H. Erdogan, and J. R. Hershey, "SDR-half-baked or well done?" in *Proc. ICASSP*, 2019, pp. 626–630.
- [24] Z. Pan, M. Ge, and H. Li, "A hybrid continuity loss to reduce over-suppression for time-domain target speaker extraction," *arXiv:2203.16843*, 2022.
- [25] D. Yu, M. Kolbæk, Z.-H. Tan, and J. Jensen, "Permutation invariant training of deep models for speaker-independent multi-talker speech separation," in *Proc. ICASSP*, 2017, pp. 241–245.
- [26] N. Zeghidour and D. Grangier, "Wavesplit: End-to-end speech separation by speaker clustering," *IEEE/ACM Trans. Audio, Speech, Lang. Process.*, vol. 29, pp. 2840–2849, 2021.
- [27] M. Maciejewski, G. Wichern, E. McQuinn, and J. Le Roux, "WHAMR!: Noisy and reverberant single-channel speech separation," in *Proc. ICASSP*, 2020, pp. 696–700.
- [28] L. Drude, J. Heitkaemper, C. Boeddeker, and R. Haeb-Umbach, "SMS-WSJ: Database, performance measures, and baseline recipe for multi-channel source separation and recognition," *arXiv:1910.13934*, 2019.
- [29] J. B. Allen and D. A. Berkley, "Image method for efficiently simulating small-room acoustics," *The Journal of the Acoustical Society of America*, vol. 65, pp. 943–950, 1979.
- [30] D. Povey, A. Ghoshal, G. Boulianne, L. Burget, O. Glembek, N. Goel, M. Hannemann, P. Motlicek, Y. Qian, P. Schwarz *et al.*, "The Kaldi speech recognition toolkit," in *Proc. Workshop ASRU*, 2011.
- [31] J. Le Roux, S. Wisdom, H. Erdogan, and J. R. Hershey, "SDR-half-baked or well done?" in *Proc. ICASSP*, 2019, pp. 626–630.
- [32] E. Vincent, R. Gribonval, and C. Févotte, "Performance measurement in blind audio source separation," *IEEE Trans. Audio, Speech, Lang. Process.*, vol. 14, pp. 1462–1469, 2006.
- [33] A. W. Rix, J. G. Beerends, M. P. Hollier, and A. P. Hekstra, "Perceptual evaluation of speech quality (PESQ)-a new method for speech quality assessment of telephone networks and codecs," in *Proc. ICASSP*, vol. 2, 2001, pp. 749–752.
- [34] J. Jensen and C. H. Taal, "An algorithm for predicting the intelligibility of speech masked by modulated noise maskers," *IEEE/ACM Trans. Audio, Speech, Lang. Process.*, vol. 24, pp. 2009–2022, 2016.
- [35] N. S. Dettelsen, J. Borovec, J. Schock, A. H. Jha, T. Koker, L. Di Liello, D. Stancil, C. Quan, M. Grechkin, and W. Falcon, "TorchMetrics-measuring reproducibility in pytorch," *Journal of Open Source Software*, vol. 7, p. 4101, 2022.
- [36] Z.-Q. Wang, "ESPnet2 pretrained model," 2023. [Online]. Available: <https://doi.org/10.5281/zenodo.7565926>
- [37] L. Zhang, Z. Shi, J. Han, A. Shi, and D. Ma, "FurcaNeXt: End-to-end monaural speech separation with dynamic gated dilated temporal convolutional networks," in *Proc. MultiMedia Modeling*. Springer, 2020, pp. 653–665.
- [38] E. Tzinis, Z. Wang, and P. Smaragdis, "Sudo Rm-Rf: Efficient networks for universal audio source separation," in *Proc. MLSP*, 2020, pp. 1–6.
- [39] Y. Zhu, X. Zheng, X. Wu, W. Liu, L. Pi, and M. Chen, "DPTCN-ATPP: Multi-scale end-to-end modeling for single-channel speech separation," in *2021 5th International Conference on Communication and Information Systems (ICCIS)*, 2021, pp. 39–44.
- [40] M. W. Lam, J. Wang, D. Su, and D. Yu, "Sandglassnet: A light multi-granularity self-attentive network for time-domain speech separation," in *Proc. ICASSP*, 2021, pp. 5759–5763.
- [41] L. Yang, W. Liu, and W. Wang, "TFPSNet: Time-frequency domain path scanning network for speech separation," in *Proc. ICASSP*, 2022, pp. 6842–6846.
- [42] J. Rixen and M. Renz, "SFSRNet: Super-resolution for single-channel audio source separation," in *Proc. AAAI Artificial Intelligence*, vol. 36, 2022, pp. 11 220–11 228.
- [43] —, "QDPN: Quasi-dual-path network for single-channel speech separation," in *Proc. Interspeech*, 2022, pp. 5353–5357.
- [44] S. Zhao and B. Ma, "MossFormer: Pushing the performance limit of monaural speech separation using gated single-head transformer with convolution-augmented joint self-attentions," in *Proc. ICASSP*, 2023, pp. 1–5.



- [45] Y. Luo, Z. Chen, and T. Yoshioka, "Dual-path RNN: efficient long sequence modeling for time-domain single-channel speech separation," in *Proc. ICASSP*, 2020, pp. 46–50.
- [46] Z.-Q. Wang, P. Wang, and D. Wang, "Multi-microphone complex spectral mapping for utterance-wise and continuous speech separation," *IEEE/ACM Trans. Audio, Speech, Lang. Process.*, vol. 29, pp. 2001–2014, 2021.
- [47] Z.-Q. Wang, G. Wichern, and J. Le Roux, "Convolutional prediction for reverberant speech separation," in *Proc. WASPAA*, 2021, pp. 56–60.
- [48] Y. Luo, Z. Chen, N. Mesgarani, and T. Yoshioka, "End-to-end microphone permutation and number invariant multi-channel speech separation," in *Proc. ICASSP*, 2020, pp. 6394–6398.
- [49] J. Zhang, C. Zorilă, R. Doddipatla, and J. Barker, "On end-to-end multi-channel time domain speech separation in reverberant environments," in *Proc. ICASSP*, 2020, pp. 6389–6393.
- [50] X. Li and R. Horaud, "Narrow-band deep filtering for multichannel speech enhancement," *arXiv:1911.10791*, 2019.
- [51] K. Tesch and T. Gerkmann, "Insights into deep non-linear filters for improved multi-channel speech enhancement," *IEEE/ACM Trans. Audio, Speech, Lang. Process.*, vol. 31, pp. 563–575, 2022.
- [52] Y. Yang, C. Quan, and X. Li, "Mcnet: Fuse multiple cues for multichannel speech enhancement," in *Proc. ICASSP*, 2023, pp. 1–5.
- [53] S. Wang, X. Kong, X. Peng, H. Movassagh, V. Prakash, and Y. Lu, "DASFormer: Deep alternating spectrogram transformer for multi/single-channel speech separation," in *Proc. ICASSP*, 2023, pp. 1–5.